Computers in Biology and Medicine 104 (2019) 43–51

Contents lists available at ScienceDirect

Computers in Biology and Medicine

journal homepage: www.elsevier.com/locate/compbiomed

An analytical method to create patient-specific deformed bone models using X-ray images and a healthy bone model

M. Kerem Ün[a,b,*], Ercan Avşar[a], İbrahim D. Akçalı[c]

[a] Department of Electrical and Electronics Engineering, Çukurova University, 01330, Sarıçam, Adana, Turkey
[b] Department of Biomedical Engineering, Çukurova University, 01330, Sarıçam, Adana, Turkey
[c] MACTIMARUM Research and Application Center, Çukurova University, 01330, Sarıçam, Adana, Turkey

ARTICLE INFO

Keywords:
3D bone modeling
Patient-specific bone models
Deformity
External fixation
Free form deformation
Mathematical modeling

ABSTRACT

Generation of patient-specific bone models from X-ray images is useful for various medical applications such as total hip replacement, implant manufacturing, knee kinematic studies and deformity correction. These models may provide valuable information required for a more reliable operation. In this work, we propose a new algorithm for generating patient-specific 3D models of femur and tibia with deformity, using only a generic healthy bone model and some simple measurements taken on the X-ray images of the diseased bone. Using the X-ray measurements, an interpolation function (a polynomial or a cubic spline) is fit to the mid-diaphyseal curve of the actual bone and the generic bone model is deformed in the guidance of this function with free form deformation method. The created models are intended to be used mainly for the visualization of fixation procedure in software-supported external fixation systems. An error measure is defined to quantify the error in this matching procedure. The method is found to be capable of producing deformed tibia models that satisfactorily reflect the actual bones, as confirmed by two orthopaedic surgeons who use software-supported external fixation systems regularly.

1. Introduction

Surgery planning plays an important role in certain orthopaedic applications such as deformity correction and limb lengthening. In order to ensure a reliable treatment, orthopaedists generally use two X-ray radiographs of the bone taken in anterior-posterior (AP) and medial-lateral (L) directions. They take certain measurements on these radiographs to plan the surgery for bone lengthening and deformity correction performed through external fixation [1]. To minimize the risk of human error, software systems are available where digital radiographs of the patient are processed semi-automatically. The software prescribes a course of treatment with an external fixator based on the information obtained from the radiographs. The external fixator used in these operations is a hexapod robotic frame attached to the bone fragments which is adjusted daily according to the treatment plan. These software systems have certain constraints with respect to the initial attachment of the robotic frame to the bone fragments and possess typically limited graphic capabilities.

In a previous study, we proposed a simple method to generate a patient-specific, morphologically normal (i.e. undeformed) bone model by processing the digital X-ray data of the patient and a generic healthy bone model [2]. A related novel graphical user interface, with the underlying mathematical theory, was also detailed in the same study. The advantages of this software over the equivalent commercially-available software systems [3,4] were explained, one being its capability of displaying a patient-specific bone-fixator model and animating the computed treatment course. Consequently, the algorithm to create a patient-specific model from a generic bone model was illustrated for cases where bones were free of any deformity but may require lengthening.

In this work, as an extension of our earlier work [2], we propose a simple algorithm to create a patient-specific model for a bone with deformity, something that has not been done before. The method relies on a generic bone model, AP and L X-ray images and some very basic measurements performed on these radiograps. The eventual goal is to use the created deformed bone model for the visualization of the patient-specific bone in the deformity correction treatment using the software system described earlier.

2. Background

3D reconstruction of a patient-specific bone model can be achieved in different ways. The most obvious way involves processing and

* Corresponding author. Department of Electrical and Electronics Engineering, Çukurova University, 01330, Sarıçam, Adana, Turkey.
E-mail addresses: unk_tr@yahoo.com (M.K. Ün), ercanavsar@gmail.com (E. Avşar), idakcali@gmail.com (İ.D. Akçalı).

https://doi.org/10.1016/j.compbiomed.2018.11.003
Received 11 July 2018; Received in revised form 20 October 2018; Accepted 3 November 2018

segmenting a sequence of slice images obtained through computed tomography (CT) or magnetic resonance imaging (MRI), and combining them to a 3D surface model [5–7]. The fact that the patient is exposed to a relatively high dosage of radiation (in the case of CT) and the high cost of the imaging are the main drawbacks of these methods. It should be also noted that, besides its clinical drawbacks, 3D reconstruction from slice data is computationally demanding as well.

Conventional X-ray is still the preferred imaging method for orthopaedic treatments requiring fixation, and CT or MR imaging is usually not performed in these procedures. As a result, researchers have tried to come up with methods to create bone models using data obtained from X-ray only. In one such study [8], transverse cross-sections of the bone are approximated with ellipses based on the information gathered from the X-rays, which are then connected to form a 3D bone model. Later works usually assume some level of *a priori* knowledge about the bone geometry. While the corresponding literature is vast, one significant distinction that can be made for these methods is whether they involve *a priori* analyses of multiple bone samples, or use a single generic bone model to create the model of the target patient-specific bone. The former methods typically utilize *statistical shape modeling* [9–15]. In statistical shape models, in order to assess the shape variability of the bone of interest, a large number of bone samples has to be evaluated to create a statistics of geometric variations in the bone "population". This usually involves generating a detailed surface mesh for each bone model, the determination of the most variable (hence most distinguishing) geometric features among models through principal components analysis and often the creation of an "average" model by using this information. Next, the average model is matched to the geometry of the actual bone, as captured from the X-ray images, through non-rigid registration. In order to simplify the problem, researchers sometimes take some recognizable geometric features of the bone (femur neck shaft angle, femoral head radius etc.) as their independent variable and correlate other geometric parameters to those [16–20]. Statistical shape modeling approach has been used in the modeling of the whole bone as well as partial bone, especially to generate models for proximal femur due to its biomechanical significance and complex shape [13,16,21,22]. While sophisticated, statistical models can be relatively complex and always require a significant amount of *a priori* data processing and a high amount of computation.

Other methods that do not use a statistical approach may still require a high amount of *a priori* data collection/processing. For example, 2D and/or 3D images of several samples of the bone of interest could be stored in an anatomical database where the best matching model to X-ray contours of the actual bone is sought for. Then, this model is deformed to obtain a closer match with the geometric parameters and landmark points of the actual bone as observed on the X-rays [23,24].

Generic-model-based methods rely on deforming a generic bone model in such a way that its virtual X-rays match the orthogonal X-rays of the actual bone as closely as possible. Unlike to statistical shape modeling, such approaches do not require *a priori* analysis of the "bone population" in order to capture the statistical variations of geometric features and, as a result, are computationally more efficient. The simplest possible approach involves a constant linear scaling to be applied to the entire generic model [25]. A variable scale factor can also be imposed on different transverse sections of the generic bone in order to match it to the actual bone [2,26]. A more sophisticated approach is based on matching some anatomical landmarks of the generic bone to the same landmarks on the actual X-ray images [27].

The method presented in this work also utilizes a generic bone model obtained from a healthy bone. The generic model is deformed through free form deformation which is utilized by many of the works cited above and explained in detail in Section 4.

3. CORA method and surgery planning

For deformity correction, surgeons usually locate a point called *center of rotation of angulation* (CORA) on the X-ray images of the patient as a part of surgery planning. To achieve that, either anatomic or mechanical axis of the treated bone is appropriately drawn through both proximal and distal ends of the bone on the X-ray images. In a bone with deformity, these two lines are not parallel and their intersection point is defined as the CORA [1]. CORA indicates the location of the surgical intervention to the deformed bone.

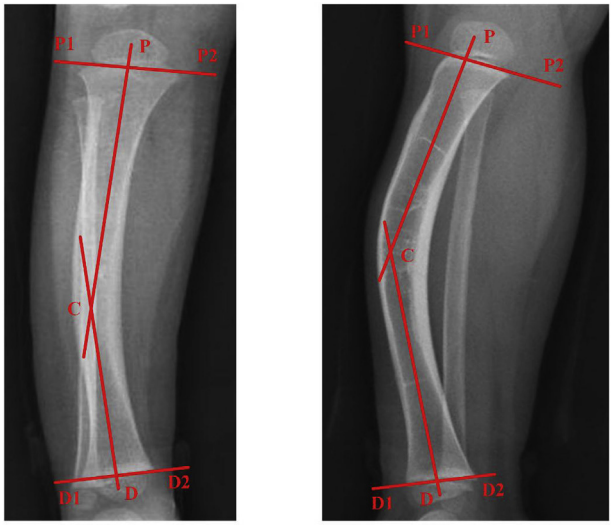

Fig. 1. Tibial anatomic axis planning on AP (a) and L (b) views of X-ray images.

CORA is located by the clinician independently on the frontal (AP) and the sagittal (L) X-ray images. Regardless of the bone type (tibia or femur), mid-diaphyseal lines (PC and CD in Fig. 1) and joint orientation lines (P_1P_2 and D_1D_2 in Fig. 1) are drawn on X-ray images and the CORA is found. For our purposes, the intersection points of mid-diaphyseal lines with joint orientation lines also have to be marked. The method to generate the 3D model of the bone involves using the information conveyed only by these lines. This approach is more practical as the clinician does not have to make any extra other measurements or markings on the X-ray images.

4. Free form deformation

To scale and deform the generic bone model to the shape of the actual bone, we have used an algorithm called *free form deformation* (FFD). The concept of FFD is often intuitively explained with the following plastic object analogy: The object to be deformed is embedded in a transparent plastic block. When the plastic block is deformed, the embedded object itself will also deform. So, the control over the plastic block allows the control of the embedded object indirectly.

Mathematically, FFD is a mapping performed through Bernstein polynomial [28]. A parametric coordinate system (s,t,u) with $0 \le s \le 1$, $0 \le t \le 1$, $0 \le u \le 1$ is introduced to enclose the entire region to be deformed. Then, $l+1$, $m+1$ and $n+1$ control points along s, t and u directions, respectively, are defined to form a grid enclosing the region. (The number of control points in each direction is user-defined.) A displacement is imposed on the control points according to the deformation to be applied on the body. Let (x_i, y_i, z_i) be the Cartesian coordinates of the ith control point after deformation. Then, a vertex in the body with the initial parametric coordinates (s_v, t_v, u_v) will be displaced to the Cartesian coordinates (x_v, y_v, z_v) after deformation according to:

$$x_v = \sum_{i=0}^{l} B_i^l(s_v) x_i \tag{1}$$

$$y_v = \sum_{i=0}^{m} B_i^m(t_v) y_i \tag{2}$$

$$z_v = \sum_{i=0}^{n} B_i^n(u_v) z_i \tag{3}$$

where B_a^b is the ath Bernstein basis polynomial of order b, defined as

$$B_a^b(t) = \binom{b}{a} t^a (1-t)^{b-a} \tag{4}$$

where $\binom{b}{a}$ indicates the binomial coefficients. This approach imposes a weighted-average displacement on a vertex, where a control point closer to the vertex has a stronger effect on its displacement. FFD produces a deformed object with a certain level of smoothness, which is an important requirement in this work to obtain a proper deformed bone model. In the developed bone reconstruction algorithm, FFD is utilized for two different purposes: Scaling the generic bone model in transverse direction (thickness matching) and deforming the generic bone model.

5. Generation of patient-specific bone models

5.1. Introduction

The shape and size of the treated bone, especially in the case of a deformity, change significantly from one patient to the other. We propose to create a 3D model of the bone by manipulating an available generic bone model to obtain the shape of the patient-specific bone. Beside the natural variations present in the geometric features of the bone, age of the patient and type of the deformity are the main determining factors for the shape and size of the bone. The algorithm presented here is aimed at modeling bones with biplanar deformities and does not change with patient's age or natural variations in bone features.

Like any reconstruction method that relies on biplanar (AP and L) X-ray views, the proposed algorithm does not take axial deformity into account. It will produce some extra error if axial deformity is also present in the bone. Similarly, in the case of axial deformity, the information gathered from AP and L images would not be sufficient to prescribe a treatment with software supported fixation systems. In this case, the axial deformity has to be quantified through clinical examination of the patient and this information has to be input to the fixation software.

5.2. Creation of generic models

The generic bone models originate from healthy bones and can be obtained through different means. In this study, the utilized tibia model is formed by combining the tibial slice images, obtained from CT scan of a cadaver, into a surface model using the CATIA software (Vélizy-Villacoublay, France). The contours of the cortical bone are drawn by hand on each slice image to ensure the smoothness of the final model. The femur model, on the other hand, has been created by scanning a cadaveric bone via David 3D Scanner system (Bonn, Germany). Both surface models basically consist of a set of vertices with triangular connectivity.

The resulting model files for both bones are relatively large, containing vertices as many as in the order of 10000's. For ease of manipulation, these large models are downscaled to smaller ones using MeshLab software (MeshLab, 2018). The total number of vertices of a typical downscaled model is in the order of 1000's.

It should be noted that a generic model serves merely as a template to obtain the deformed bone model. It is important that the model is geometrically smooth such that after scaling and FFD it stays smooth.

5.3. Model manipulation

The deformed model is created through four steps that are applied separately to AP and L views. The first three steps are straightforward and described in detail in our previous work [2]. Basically, they involve obtaining the projection of the generic bone model in the AP and L directions, the detection of the edges of the actual bone on the X-ray images and scaling the generic model along axial and transverse directions according to the bone image. The final step involves deforming the scaled generic bone to the actual bone, which is described in detail below.

5.4. Deforming the generic model

The procedure starts with fitting a curve to the midline of the actual bone on the X-ray images, which is done separately in AP and L views. To achieve that, a coordinate system is defined on the AP and L images (Fig. 1) where the origin is located on the CORA, and the coordinates of points P and D are defined accordingly. The fitted curves are expected to overlap with the midline of the deformed bone in both views while satisfying certain constraints at the bone ends. The curves provide a quantification of the bone shape which is then used within FFD to deform the generic bone model to the actual bone. Two different curve fitting approaches, namely polynomial and spline interpolations, have been tried in this work.

5.4.1. Fourth order polynomial interpolation

In this method, the mid-diaphyseal curve connecting the points P and D is interpolated with a fourth order polynomial. The point e is the intercept of this curve with the line bisecting the angle between the line segments PC and CD (Fig. 2).

The five coefficients of the fitted general fourth order polynomial, namely

$$p(x) = a_1x^4 + b_1x^3 + c_1x^2 + d_1x + e_1 \tag{5}$$

can be uniquely determined by using the constraints:

i) $p(D_x) = D_y$
ii) $p(P_x) = P_y$
iii) $p(e_x) = e_y$
iv) $p'(D_x) = -1/m_d$
v) $p'(P_x) = -1/m_p$

The first three constraints ensure that the fitted curve passes through the points D, P and e. The last two constraints make sure that the curve intersects the joint orientation lines P_1P_2 and D_1D_2 at right angles, where m_p and m_d are the slopes of the proximal P_1P_2 and distal D_1D_2 joint orientation lines, respectively. To find the coefficients, a system of five equations in five unknowns is solved, which can be written in matrix form as:

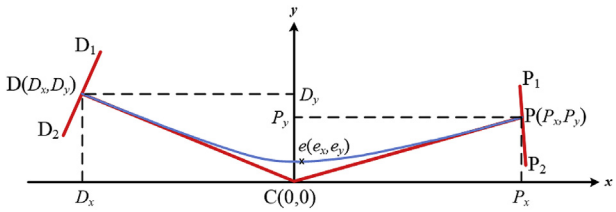

Fig. 2. The anatomic axes and joint orientation lines (red lines), and the fitted fourth order polynomial (blue curve).

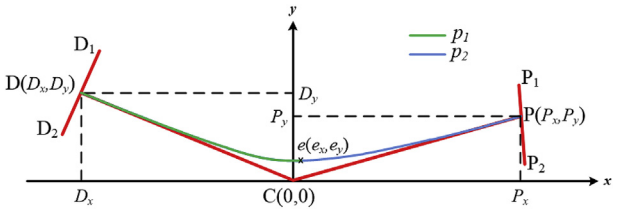

Fig. 3. The anatomic axes and joint orientation lines (red lines), and the fitted cubic splines (green and blue curves).

$$\begin{pmatrix} D_x^4 & D_x^3 & D_x^2 & D_x & 1 \\ P_x^4 & P_x^3 & P_x^2 & P_x & 1 \\ e_x^4 & e_x^3 & e_x^2 & e_x & 1 \\ 4D_x^3 & 3D_x^2 & 2D_x & 1 & 0 \\ 4P_x^3 & 3P_x^2 & 2P_x & 1 & 0 \end{pmatrix} \begin{pmatrix} a_1 \\ b_1 \\ c_1 \\ d_1 \\ e_1 \end{pmatrix} = \begin{pmatrix} D_y \\ P_y \\ e_y \\ -1/m_d \\ -1/m_p \end{pmatrix} \tag{6}$$

5.4.2. Cubic splines interpolation

In this method, the path between the points P and D is interpolated with a cubic spline (Fig. 3).

Two subintervals are defined between D_x-e_x and e_x-P_x value pairs along the x-axis. The corresponding cubic interpolating polynomials in each interval are defined, respectively, as:

$$p_1(x) = a_1x^3 + b_1x^2 + c_1x + d_1 \tag{7}$$

$$p_2(x) = a_2x^3 + b_2x^2 + c_2x + d_2 \tag{8}$$

whose coefficients are to be determined according to the constraints:

i) $p_1(e_x) = e_y$
ii) $p_2(e_x) = e_y$
iii) $p_1(D_x) = D_y$
iv) $p_2(P_x) = P_y$
v) $p'_1(e_x) = p'_2(e_x)$
vi) $p''_1(e_x) = p''_2(e_x)$
vii) $p'_1(D_x) = -1/m_d$
vii) $p'_2(P_x) = -1/m_p$

The first two constrain ensure the continuity of the spline across the transition point e. The next two make sure that the spline passes through the points P and D. The constraints *(v)* and *(vi)* enforce the continuity of the first and second derivatives of the spline across the transition point e. Finally, the last two conditions constrain the slope of the spline at points D and P such that it intersects the joint orientation lines at right angles. As in the case of polynomial curve fit, m_p and m_d are the slopes of the lines P_1P_2 and D_1D_2, respectively. The spline coefficients are found by solving the related equation system in eight unknowns, written in matrix form as:

$$\begin{pmatrix} e_x^3 & e_x^2 & e_x & 1 & 0 & 0 & 0 & 0 \\ 0 & 0 & 0 & 0 & e_x^3 & e_x^2 & e_x & 1 \\ D_x^3 & D_x^2 & D_x & 1 & 0 & 0 & 0 & 0 \\ 0 & 0 & 0 & 0 & P_x^3 & P_x^2 & P_x & 1 \\ 3e_x^2 & 2e_x & 1 & 0 & -3e_x^2 & -2e_x & -1 & 0 \\ 6e_x & 2 & 0 & 0 & -6e_x & -2 & 0 & 0 \\ 3D_x^2 & 2D_x & 1 & 0 & 0 & 0 & 0 & 0 \\ 0 & 0 & 0 & 0 & 3P_x^2 & 2P_x & 1 & 0 \end{pmatrix} \begin{pmatrix} a_1 \\ b_1 \\ c_1 \\ d_1 \\ a_2 \\ b_2 \\ c_2 \\ d_2 \end{pmatrix} = \begin{pmatrix} e_y \\ e_y \\ D_y \\ P_y \\ 0 \\ 0 \\ -1/m_d \\ -1/m_p \end{pmatrix} \tag{9}$$

5.4.3. Generic model deformation using the interpolating functions

The deformation algorithm matches the midline of the generic bone with the midline of the deformed bone both in AP and L views (Fig. 4). Furthermore, it is made sure that every transverse plane in the generic bone model transforms to a plane that is perpendicular to the fitted curve in the deformed bone model. (In other words, the generic model is "bent" to the deformed model.). This involves a rotation and a translation to be applied to the generic bone geometry using FFD. The procedure is performed separately in the AP and L planes.

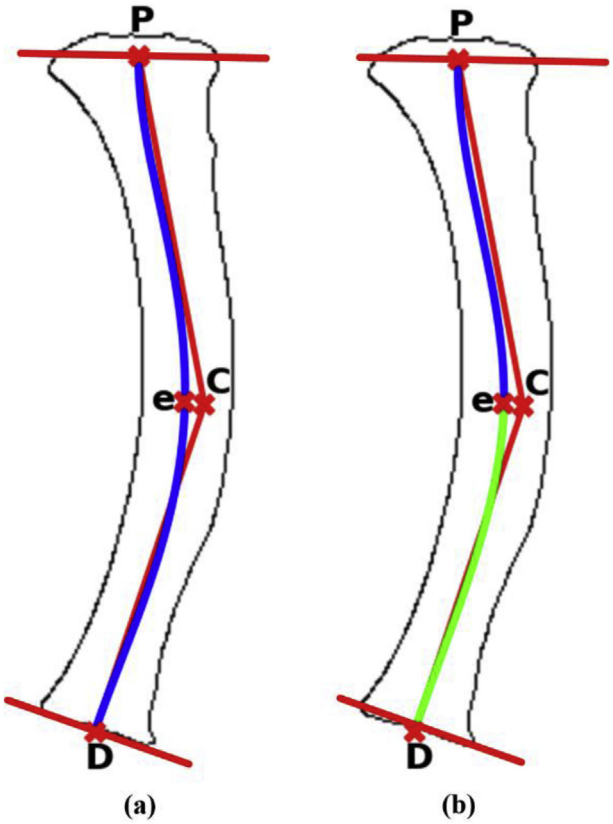

Fig. 4. Functions obtained with fourth order polynomial fit (a) and cubic splines fit (b) superposed on the edge images.

After the polynomial or spline expression is obtained for the bone midline curve (Sections 5.4.1 and 5.4.2), control points of the FFD space enclosing the generic bone model are displaced according to the curve equation.

Magnitudes of the rotations and translations are determined with the help of the fitted curve. A control point $A(x_A, y_A, z_A)$ is translated in x-direction according to the value of $p(x_A)$ (or $p_1(x_A)$ or $p_2(x_A)$ in the case of spline interpolation). As for the rotation, the transverse plane that passes through $A(x_A, y_A, z_A)$ projects as the line $x = x_A$ on AP and L views, and this line is rotated such that it becomes perpendicular to the fitted curve at $x = x_A$ after deformation. The rotation angle ϕ in the considered transverse plane can be found by evaluating $p'(x_A)$ value (or, $p'_1(x_A)$ or $p'_2(x_A)$ in the case of spline interpolation). At a general x level, it is equal to

$$\phi = \tan^{-1}\left(\frac{-1}{p'(x)}\right) \tag{10}$$

For practical purposes, rotation is performed first, followed by translation. In AP and L views, the calculated rotation is performed about the point $(x, 0)$. Following that, all control points on that rotated plane are translated by the amount $p(x)$. A sample deformed model obtained through this procedure is shown in Fig. 5.

The deformation procedure is done first in AP and then in L views. In other words, the generic bone is deformed first in AP, then in L planes. Note that the rotation operation is mathematically not commutative, in general. Theoretically, there may be a difference in the outcome if the rotation is performed first in L, then in AP view. However, since rotation angles involved in the deformation procedure

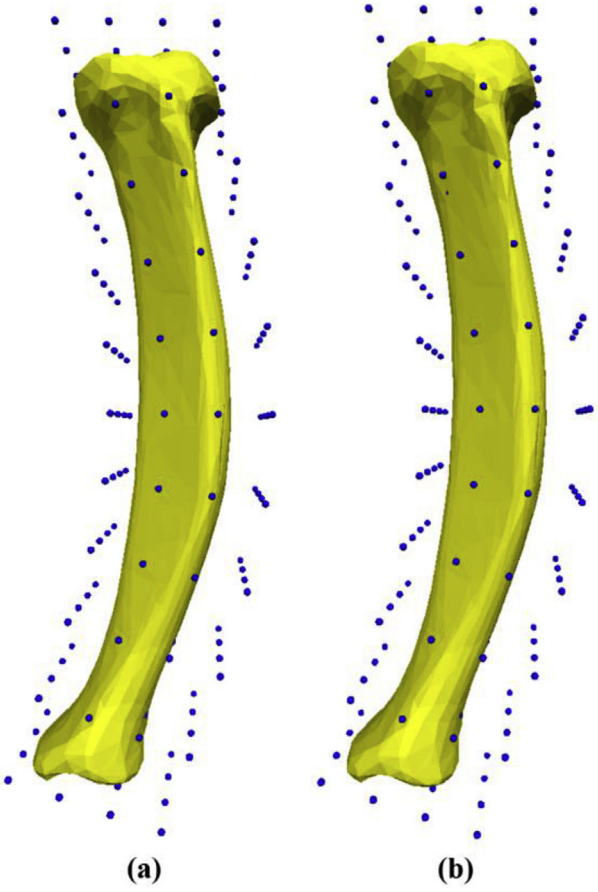

Fig. 5. The generic bone models after deformation according to the fourth order polynomial (a) and the cubic splines (b). The dots indicate the control points enclosing the bone geometry.

are relatively small, the difference is negligible.

5.5. Error calculation

To evaluate the performance of the deformation algorithm, the simple error measure proposed in the preceding work [2] is utilized here, too. In our study, the ideal situation would be an exact overlap AP and L silhouettes of the created model with the AP and L X-ray views of the treated bone as observed by the clinician. Hence, we have based our error measure on the distance between the boundary point of the transformed generic bone image and the corresponding point on the boundary of the actual bone on the X-ray image (Fig. 6). The distance, denoted as l, is measured on n boundary point pairs giving a *total error* E_{total} expressed as:

$$E_{tot} = \sum_{i=1}^{n} l_i \tag{11}$$

and an *average error* E_{ave} as:

$$E_{ave} = \frac{E_{total}}{n} \tag{12}$$

A normalized *error*, E_{norm} is defined as

$$E_{norm} = \frac{E_{ave}}{W} \tag{13}$$

where W is the maximum width of the bone, to have a dimensionless error measure that is independent of the bone size. In that respect, an E_{norm} value of, say, 0.1 corresponds to a hypothetical situation where all measurement points of the transformed generic bone image lie $0.1 \cdot W$ (10% of the maximum width) away from the corresponding point on the actual bone image.

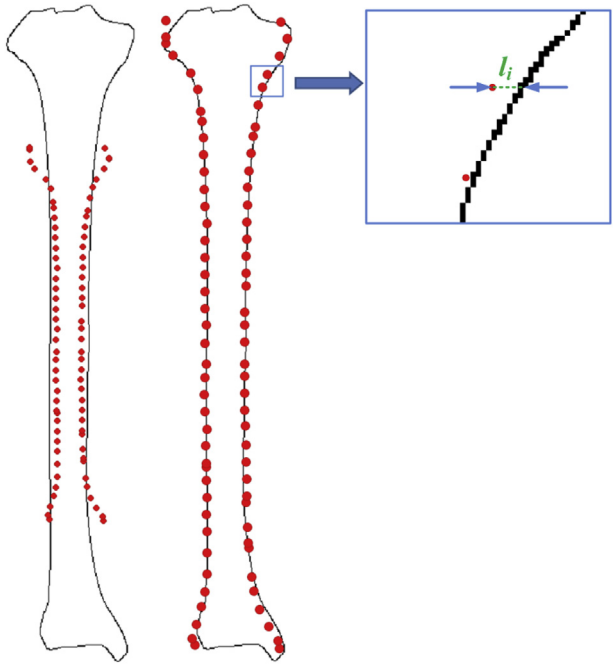

Fig. 6. Superposed images of actual bone and generic bone in AP view before (left) and after scaling (right). The error in the matching procedure is measured using the distances l_i.

5.6. Examples

The proposed algorithm for the creation of the actual bone model from the generic model has been tested on nine tibia and two femur image sets obtained from Orthopaedics and Traumatology Department, Faculty of Medicine, Cukurova University.

Before presenting the examples, an exception related with generic femur model should be explained here. The L view of a healthy femur bone is not straight like tibia. In this view, a healthy femur has an angle of about 10° between the proximal and distal mid-diaphyseal lines [1]. Since the proposed algorithm is based on a straight bone axis, this angulation in the sagittal plane should be fixed before the deformed femur model can be created. We have manually corrected this angulation in the generic bone using FDD.

The FFD grid, where bone models are deformed, has $3 \times 21 \times 3$ control points along x, y and z directions, respectively. Once the control points of the grid are rotated and translated using Eqs. (5), (7), (8) and (10), all vertices of the generic model move to their deformed coordinates.

6. Results

Typical results comparing the actual bone with the deformed generic model are shown in Figs. 7–10. In particular, X-ray images of one actual tibia (Tibia #1) and its X-ray contour is compared with the corresponding deformed generic model and its projection, respectively, in the AP and L views in Figs. 7–8. A similar comparison is made for an actual femur (Femur #1) in Figs. 9–10. For all deformed bone images analyzed, the average and normalized error made in matching the generic bone model to the actual bone in both AP and L views are listed in Table 1 for polynomial interpolation and Table 2 for spline interpolation. The first thing to notice is that there is no appreciable difference between models created through polynomial (Table 1) and spline interpolation (Table 2), which can be also visually observed from

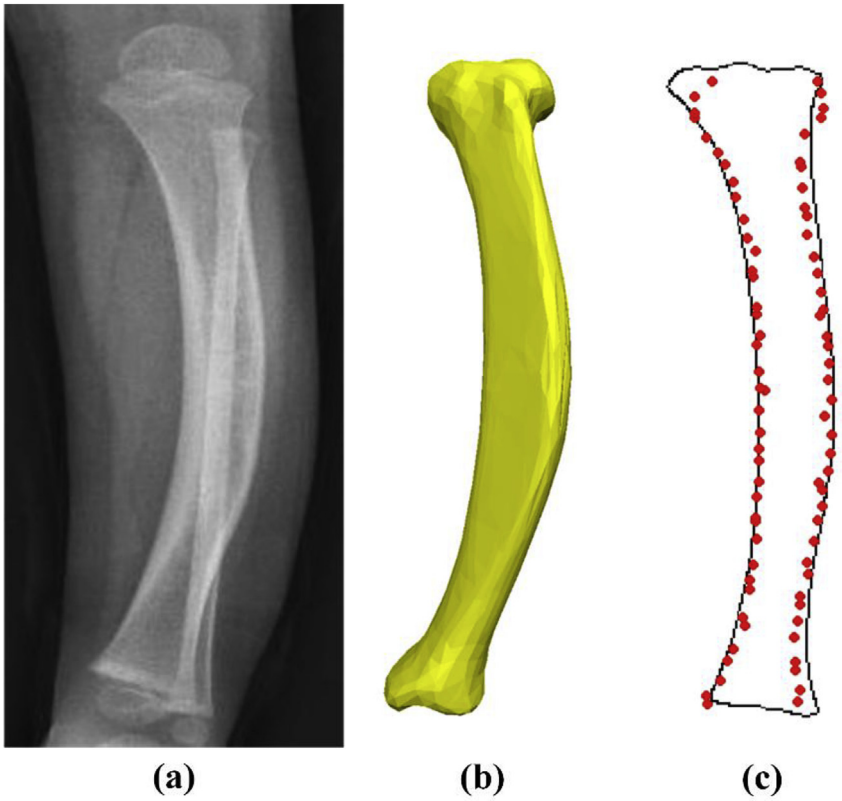

Fig. 7. (a) Actual X-ray images of a tibia in AP direction, (b) the deformed generic model, (c) contour of the actual bone (line) and projection of the deformed model (dots) (Fourth order polynomial fit).

Figs. 4–5.

For both interpolation methods, the normalized error is 0.05 (i.e. 5% of the maximum width) or less in the AP view for most tibia samples, with a model average of 0.054. This corresponds approximately to an average error of 3.8 mm for a typical tibial bicondylar width of $W = 7$ cm. Similarly, the model with the lowest error (Tibia

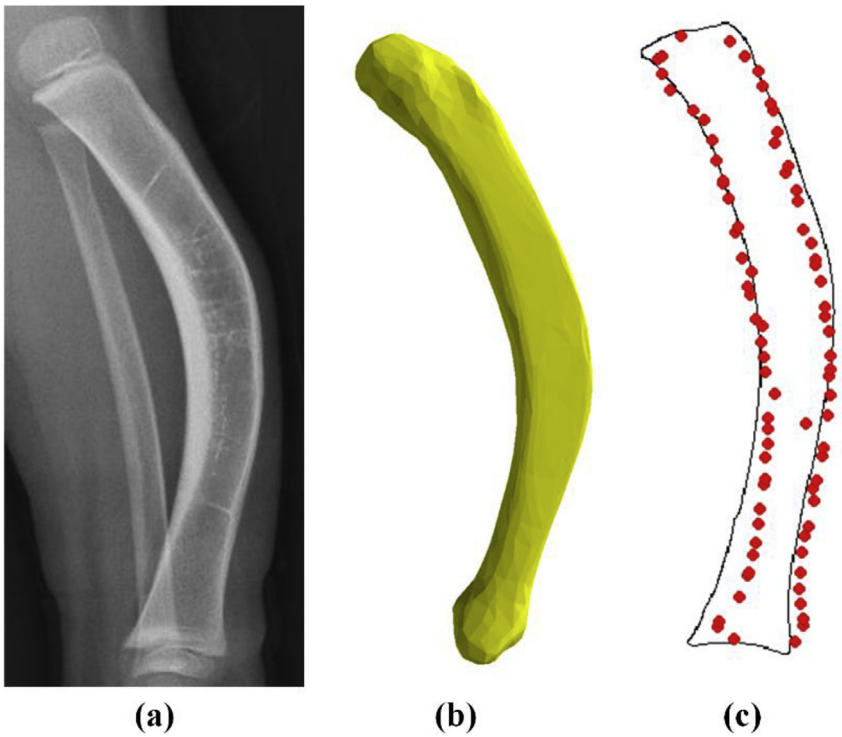

Fig. 8. a) Actual X-ray images of a tibia in L direction, (b) the deformed generic model, (c) contour of the actual bone (line) and projection of the deformed model (dots) (Fourth order polynomial fit).

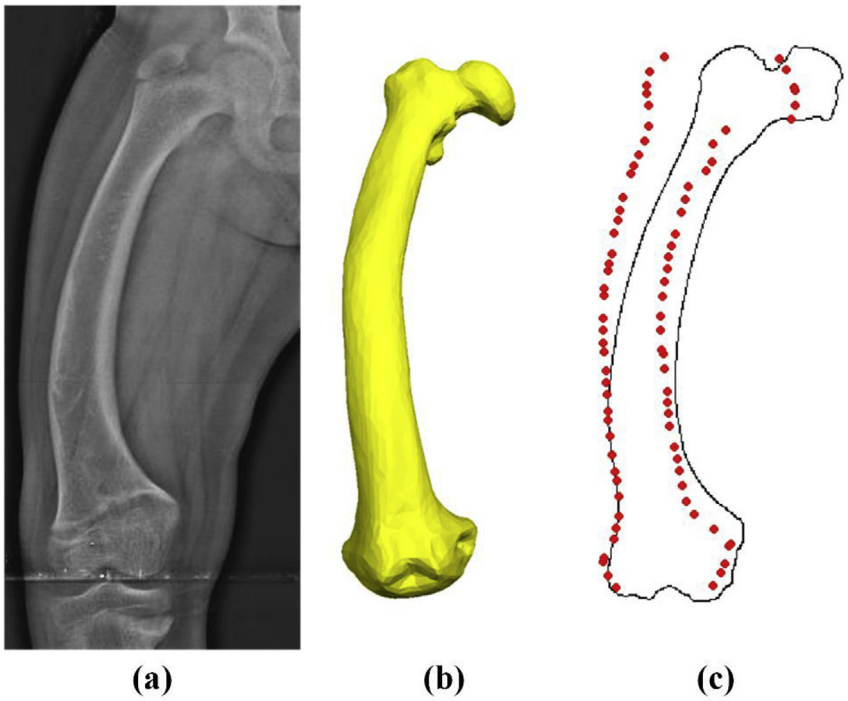

Fig. 9. a) Actual X-ray images of a femur in AP direction, (b) the deformed generic model (c) contour of the actual bone (line) and the projection of the deformed model (dots) (Fourth order polynomial fit).

#3) has an error of 2 mm. For the AP view, the average error over all tibia samples is about 0.086, which corresponds to an error of 6.0 mm for $W = 7$ cm.

For the two femur samples analyzed, the error is significantly higher than the tibia samples independent of the interpolation method. In the AP view, the normalized error can be higher than 0.13. The error in the L view is about half of this value.

7. Discussion

The method proposed in this work is unique in the sense that it is used to create the model of a morphologically abnormal (i.e. deformed) bone and utilizes the very same simple data set for model creation that the clinician uses for deformity treatment. It is based on a novel polynomial-fit algorithm. As a result, model creation is a relatively rapid computational process that is usually completed in less than a minute on a standard PC.

The method has been tried on tibia and femur samples. A higher matching error for the femur is observed due to the complex shape of the proximal femur. Unlike tibia, the error is higher in the AP view for femur, which is expected since the geometrical complexity of the bone is mainly on the AP view. These observations indicate that the proposed deformation algorithm is appropriate to model the deformed tibia, while it may require some further improvement for femur modeling to better handle the shape complexity of the proximal femur. On the other hand, software supported external fixation systems are mainly used in the correction of diaphyseal deformities where the resemblance of the diaphysis of the femur to the actual bone is more important rather than

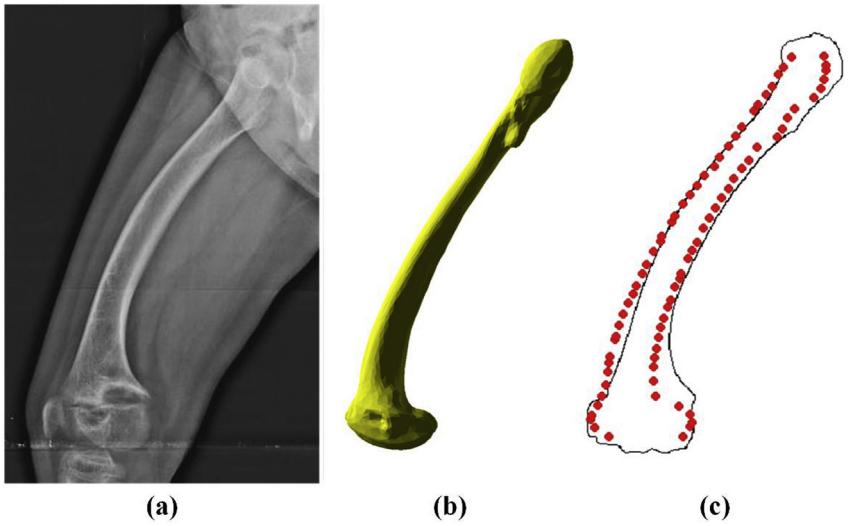

Fig. 10. a) Actual X-ray images of a femur in L direction, (b) the deformed generic model, (c) contour of the actual bone (line) and projection of the deformed model (dots) (Fourth order polynomial fit).

Table 1
Average and normalized errors calculated for the generated patient-specific deformed bone models (fourth order polynomial fit).

Samples	AP image		L image	
	E_{ave} (pixels)	E_{norm}	E_{ave} (pixels)	E_{norm}
Femur #1	13.004	0.137	6.030	0.065
Femur #2	11.664	0.134	5.864	0.066
Tibia #1	2.266	0.033	6.701	0.089
Tibia #2	3.104	0.045	6.857	0.089
Tibia #3	2.729	0.032	3.295	0.058
Tibia #4	2.730	0.033	3.697	0.066
Tibia #5	7.263	0.043	11.802	0.111
Tibia #6	8.378	0.097	5.602	0.067
Tibia #7	8.621	0.074	9.874	0.098
Tibia #8	9.068	0.075	11.576	0.118
Tibia #9	5.061	0.050	5.263	0.082

Table 2
Average and normalized errors calculated for the generated patient-specific deformed bone models (Cubic splines fit).

Samples	AP image		L image	
	E_{ave} (pixels)	E_{norm}	E_{ave} (pixels)	E_{norm}
Femur #1	12.803	0.134	5.884	0.064
Femur #2	10.968	0.126	5.751	0.064
Tibia #1	2.346	0.034	5.683	0.075
Tibia #2	3.408	0.049	5.880	0.076
Tibia #3	2.909	0.035	3.295	0.058
Tibia #4	2.822	0.034	3.696	0.066
Tibia #5	8.701	0.051	10.940	0.103
Tibia #6	6.675	0.077	4.775	0.057
Tibia #7	10.691	0.091	15.324	0.151
Tibia #8	8.019	0.067	11.621	0.118
Tibia #9	5.196	0.051	4.989	0.078

its proximal part.

The accuracy in reflecting the actual bone, required from a reconstructed bone model, is largely prescribed by the usage purpose. For example, if the objective is to perform a stress analysis on the patient-specific bone model, the generated solid model needs to have a high accuracy. In this case, smaller geometric features that may act as stress concentration spots should be captured by the modeling process for a reliable patient-specific finite element analysis. On the other hand, a lesser accuracy in the model of the target organ may be acceptable for surgical simulation and/or training. Clearly, the required accuracy in the model is one determinant for the modeling approach to be utilized. It could be also argued that the computational burden of the method generally increases with the required modeling accuracy.

The error in 3D reconstruction methods depends on the complexity of the geometric shape to be constructed, as well as on the complexity of the reconstruction algorithm. In statistical shape models, the error, measured usually as point-to-surface distance, may differ from one part of the bone to the other significantly. Generally, it could be said that the mean error is between 0.6 and 1.5 mm for femur and tibia models in statistical shape modeling [9–14,16,18]. This value range is significantly lower than 3.8 mm, our mean error for tibia. (It should be noted that, for simplicity, we have measured the error along horizontal lines, as shown in Fig. 6, which results to a higher value than the point-to-surface measurement performed perpendicular to the bone surface.) On the other hand, a statistical approach to determine the distribution of geometric parameters in an abnormal bone population is not sensible, since every deformed bone is shapewise different and unique. Hence, model creation based on the deformation of a generic bone model, such as the one presented here, is a more suitable approach compared to statistical shape modeling.

Other generic-model-based methods described in the literature give an error in the range of 0.2–1.5 mm [25,29] which is significantly smaller than the error attained in this study for tibia modeling. While those methods typically impose different deformations on different points of the generic bone boundary and often find a best match through iteration [29,30], our method imposes one type of deformation on the entire generic bone and obtain the deformed bone model directly. As a result, our method is much easier to apply, requires minimal input from the clinician and is computationally efficient in that sense. Since the reproduced model is intended to be used within an external fixation software for instant visualization and simulation of deformity correction procedure, it is more important that the model is created with minimal effort from the clinician and adequately reflects the shape of the actual bone, especially close to the site of the surgical operation. The curve fitting algorithm which is based on the location of CORA (among other points) will ensure that the modeling error is relatively low close to the surgical operation site, which is located near CORA. A qualitative evaluation done by two orthopaedic surgeons at Çukurova University, who use external fixation software systems regularly, has revealed that the model created by the proposed method satisfactorily resembles the actual bone.

8. Conclusion

In this study, a novel method for generating patient-specific deformed bone models is proposed. The algorithm entirely relies on the X-rays taken in the AP and L directions of the bone and simple presurgery measurements done by the clinician on the X-ray images. The basic idea behind the algorithm is to transform the model of a healthy bone to the patient-specific bone model using the data gathered from the X-rays. This approach is found to be computationally efficient and has performed relatively well in tibia samples.

In a previous work [2], a simple approach was described to create a patient-specific model of a bone, which had no deformity but required lengthening, to be used within an external fixation software. The underlying idea was to provide the clinician with a more realistic visual in a bone-lengthening treatment. Along the same lines, the main motivation for creating patient-specific deformed bone models in this work has been to use them within the same software to visualize deformity correction procedure (Fig. 11). Deformity correction is arguably the most important application area of software-supported external fixation systems, and it is to the benefit of the clinician to be able to visualize the model of the patient-specific deformed bone.

The method presented in this work can be furthered in a couple of aspects in the future. Shape and geometry can vary tremendously in deformed bones. Some deformities may be too severe or too irregular. In such cases, the clinician may choose to analyze the bone shape with three mid-diaphyseal lines and define two CORAs. Consequently, the mathematical model presented here can be extended to tackle a wider variety of deformities.

Femur has the most complex geometry among the long bones and, as observed in this study, modeling of deformed femur is more challenging and error prone. We believe that, the presented algorithm can be modified or an algorithm specific to femur can be developed in order to create a better patient-specific deformed femur model from the generic model.

Conflict of interest

The authors declare no conflict of interest.

Acknowledgements

This research is supported by the Turkish Research and Science Council (TÜBİTAK) under Grant No: 112M406.

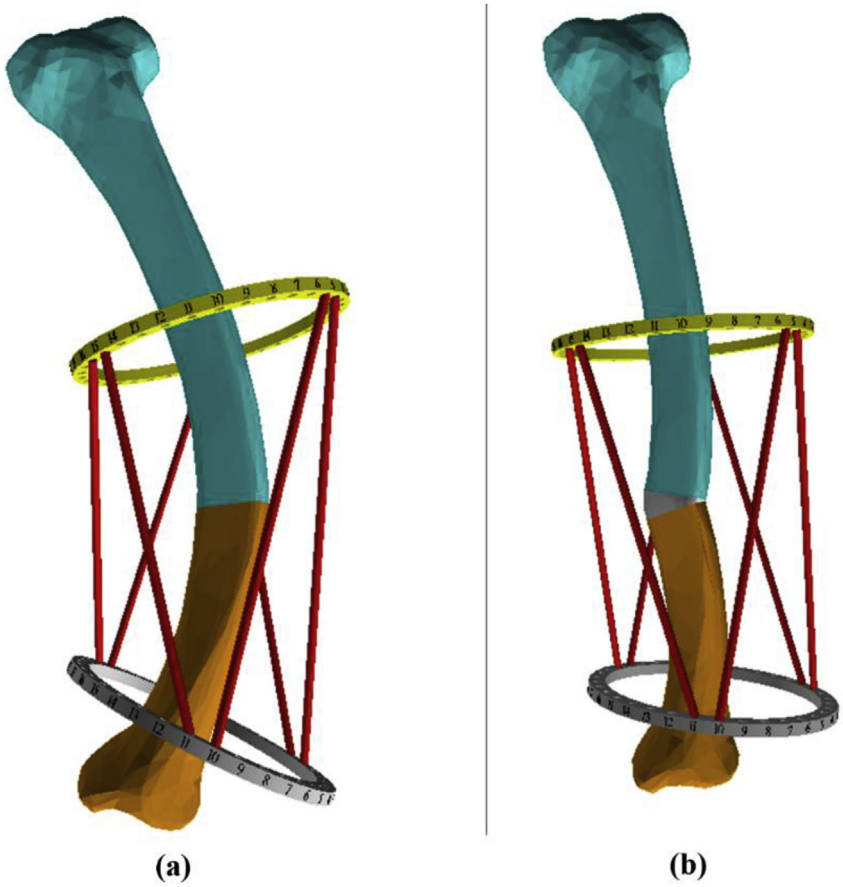

Fig. 11. The usage of a deformed tibia model for visualization of a deformity correction procedure within the previously developed software system [2]. The configuration in the beginning (a) and the end (b) of the treatment procedure.

References

[1] D. Paley, Principles of Deformity Correction, Springer, 2005.
[2] E. Avşar, K. Ün, Automatic 3D modeling and simulation of bone-fixator system in a novel graphical user interface, Informat. Med. Unlocked 2 (2016) 78–91.
[3] https://www.spatialframe.com/, Accessed on 10.07.2018.
[4] http://www.smartcorrection.com/, Accessed on 10.07.2018.
[5] M. Viceconti, C. Zannoni, D. Testi, A. Cappello, CT data sets surface extraction for biomechanical modeling of long bones, Comput. Methods Progr. Biomed. 59 (1999) 159–166.
[6] M. Viceconti, M. Davinelli, F. Taddei, A. Cappello, Automatic generation of accurate subject-specific bone finite element models to be used in clinical studies, J. Biomech. 37 (2004) 1597–1605.
[7] Z. Yosibash, N. Trabelsi, C. Milgrom, Reliable simulations of the human proximal femur by high-order finite element analysis validated by experimental observations, J. Biomech. 40 (2007) 3688–3699.
[8] L. Caponetti, A.M. Fanelli, Computer-aided simulation for bone surgery, IEEE Comput Graph 13 (1993) 86–92.
[9] A. Hurvitz, L. Joskowicz, Registration of a CT-like atlas to fluoroscopic X-ray images using intensity correspondences, Int. J. Comput. Ass. Rad. 3 (2008) 493–504.
[10] S. Benameur, M. Mignotte, H. Labelle, J.A. De Guise, A hierarchical statistical modeling approach for the unsupervised 3-D biplanar reconstruction of the scoliotic spine, IEEE T Bio-Med. Eng 52 (2005) 2041–2057.
[11] S. Schumann, R. Bieck, R. Bader, J. Heverhagen, L.P. Nolte, G.Y. Zheng, Radiographic reconstruction of lower-extremity bone fragments: a first trial, Int. J. Comput. Ass. Rad. 11 (2016) 2241–2251.
[12] N. Baka, B.L. Kaptein, M. de Bruijne, T. van Walsum, J.E. Giphart, W.J. Niessen, B.P.F. Lelieveldt, 2D-3D shape reconstruction of the distal femur from stereo X-ray imaging using statistical shape models, Med. Image Anal. 15 (2011) 840–850.
[13] R. Kurazume, K. Nakamura, T. Okada, Y. Sato, N. Sugano, T. Koyama, Y. Iwashita, T. Hasegawa, 3D reconstruction of a femoral shape using a parametric model and two 2D fluoroscopic images, Comput. Vis Image Und. 113 (2009) 202–211.
[14] S.P. Vaananen, L. Grassi, G. Flivik, J.S. Jurvelin, H. Isaksson, Generation of 3D shape, density, cortical thickness and finite element mesh of proximal femur from a DXA image, Med. Image Anal. 24 (2015) 125–134.
[15] R. Blanc, C. Seiler, G. Szekely, L.P. Nolte, M. Reyes, Statistical model based shape prediction from a combination of direct observations and various surrogates: application to orthopaedic research, Med. Image Anal. 16 (2012) 1156–1166.
[16] A. Baudoin, W. Skalli, J.A. De Guise, D. Mitton, Parametric subject-specific model for in vivo 3D reconstruction using bi-planar X-rays: application to the upper femoral extremity, Med. Biol. Eng. Comput. 46 (2008) 799–805.
[17] Y. Chaibi, T. Cresson, B. Aubert, J. Hausselle, P. Neyret, O. Hauger, J.A. de Guise, W. Skalli, Fast 3D reconstruction of the lower limb using a parametric model and statistical inferences and clinical measurements calculation from biplanar X-rays, Comput. Meth. Biomec. 15 (2012) 457–466.
[18] S. Quijano, A. Serrurier, B. Aubert, S. Laporte, P. Thoreux, W. Skalli, Three-dimensional reconstruction of the lower limb from biplanar calibrated radiographs, Med. Eng. Phys. 35 (2013) 1703–1712.
[19] V. Pomero, D. Mitton, S. Laporte, J.A. de Guise, W. Skalli, Fast accurate stereoradiographic 3D-reconstruction of the spine using a combined geometric and statistic model, Clin. Biomech. 19 (2004) 240–247.
[20] J. Thevenot, J. Koivumaki, V. Kuhn, F. Eckstein, T. Jamsa, A novel methodology for generating 3D finite element models of the hip from 2D radiographs, J. Biomech. 47 (2014) 438–444.
[21] G. Zheng, L.P. Nolte, Surface reconstruction of bone from X-ray images and point distribution model incorporating a novel method for 2D-3D correspondence, IEEE Computer Society Conference on Computer Vision and Pattern Recognition (CVPR'06)New York, NY, 2006.
[22] K.T. Rajamani, M.A. Styner, H. Talib, G.Y. Zheng, L.P. Nolte, M.A.G. Ballester, Statistical deformable bone models for robust 3D surface extrapolation from sparse data, Med. Image Anal. 11 (2007) 99–109.
[23] P. Messmer, G. Long, N. Suhm, P. Regazzoni, A.L. Jacob, Volumetric model determination of the tibia based on 2D radiographs using a 2D/3D database, Comput. Aided Surg. 6 (2001) 183–194.
[24] P.E. Galibarov, P.J. Prendergast, A.B. Lennon, A method to reconstruct patient-specific proximal femur surface models from planar pre-operative radiographs, Med. Eng. Phys. 32 (2010) 1180–1188.
[25] B. Schmutz, K.J. Reynolds, J.P. Slavotinek, Customization of a generic 3D model of the distal femur using diagnostic radiographs, J. Med. Eng. Technol. 32 (2008) 156–161.
[26] M. Gunay, M.B. Shim, K. Shimada, Cost- and time-effective three-dimensional bone-shape reconstruction from X-ray images, Int J Med Robot Comp 3 (2007) 323–335.
[27] J.W. Fernandez, P. Mithraratne, S.F. Thrupp, M.H. Tawhai, P.J. Hunter, Anatomically based geometric modelling of the musculo-skeletal system and other organs, Biomechanics Model. Mechanobiol. 2 (2004) 139–155.
[28] T.W. Sederberg, S.R. Parry, Free-form deformation of solid geometric models, SIGGRAPH Comput. Graph. 20 (1986) 151–160.
[29] P. Gamage, S.Q. Xie, P. Delmas, W.L. Xu, Diagnostic radiograph based 3D bone reconstruction framework: application to the femur, Comput. Med. Imag. Graph. 35 (2011) 427–437.
[30] K. Koh, Y.H. Kim, K. Kim, W.M. Park, Reconstruction of patient-specific femurs using X-ray and sparse CT images, Comput. Biol. Med. 41 (2011) 421–426.